JOURNAL OF AIRCRAFT
Vol. 29, No. 2, March–April 1992

Evaluation of a Navier-Stokes Prediction of a Jet in a Crossflow

Karlin R. Roth*
NASA Ames Research Center, Moffett Field, California 94035
and
Richard L. Fearn† and Siddharth S. Thakur‡
University of Florida, Gainesville, Florida 32611

The interaction between a subsonic jet exhausting perpendicularly through a flat plate into a crossflow is investigated numerically using an implicit, two-factor, partially flux split solver for the thin-layer Navier-Stokes equations. The numerical model is limited to steady and laminar flow for both the jet and crossflow. The accuracy of the method is assessed by comparing computed and experimental results for flows with jet-to-crossflow velocity ratios of 4, 6, and 8. Qualitatively, it is found that all of the global flow physics, including the jet trajectory, the contrarotating vortex pair, entrainment, and the wake region near the flat plate, are captured numerically. The computed velocity field is analyzed to determine the properties of the contrarotating vortex pair. Reasonable quantitative agreement between the computation and the experiment is found for the vortex properties as well as for the jet centerline and the plate pressure distribution. Computational flow visualization techniques are used to provide insight into the physics of the three-dimensional flowfield.

Nomenclature

C_p	=	pressure coefficient, $(p - p_\infty)/0.5\rho_\infty u_\infty^2$
D	=	jet diameter, in.
M	=	Mach number
p	=	fluid pressure, lb/ft^2
$\boldsymbol{Q}$	=	vector of conservative variables
R	=	effective velocity ratio, M_j/M_∞
Re	=	Reynolds number, $\rho_\infty u_\infty D/\mu$
t	=	time, s
u,v,w	=	Cartesian velocity components, ft/s
x,y,z	=	Cartesian coordinates normalized by jet diameter
Γ	=	circulation, in.^{2}/s
μ	=	fluid viscosity, lb/ft-s
ξ,η,ζ,τ	=	computational variables
ρ	=	fluid density, slugs/ft^3
φ	=	cross-sectional inclination angle, deg

Subscripts

c	=	jet centerline
i,j,k	=	grid indices
j	=	jet exit conditions
max	=	maximum
min	=	minimum
v	=	local coordinate system based on the vortex location
∞	=	freestream condition

Introduction

DURING the transition from hover to wing-borne flight, short takeoff and vertical landing (STOVL) aircraft rely on the direct thrust of lift jets to supplement for aerodynamic lift. The interaction of the lift jets with the flow over the aerodynamic surface produces a complex, three-dimensional flowfield around the aircraft. This interaction is due to jet blockage, entrainment, separation of the wake, and lift-induced vortices. In comparison with the linear addition of wing lift and jet lift without interference, the interaction usually causes a loss of lift and an increment of nose-up pitching moment, both of which tend to increase with forward flight velocity.[1]

The application of computational fluid dynamics to the powered lift problem is evaluated in this study. As a logical step toward the analysis of a complete STOVL aircraft throughout its entire flight regime, a simpler flowfield that isolates the physics of the jet/freestream interaction is investigated. The problem considered is a round subsonic jet exhausting perpendicularly through a large flat plate into a subsonic crossflow. This configuration retains the physics of the aerodynamic/propulsive interaction problem without the added complexity of the aircraft geometry, engine inlet flows, ground effects, and multiple jets.

The subsonic jet in a crossflow has been studied extensively, both by experiment and by analysis, as reviewed in Refs. 2–7. Many experimental investigations, for example, Refs. 8–17, focused on determining the jet trajectory and the plate pressure distribution and on describing the contrarotating vortex pair. Finer scale flow features, such as the separated region upstream of the jet, the jet development close to the exit, and the detailed wake structure, have also been measured for selected jet and freestream conditions.[18–21] A sketch of the global flow features, which is based on the qualitative description presented by Fearn[22] and shown in Fig. 1, sets forth the various regions of the jet plume together with the wake region near the plate downstream of the jet orifice. These properties of a jet in a crossflow depend primarily on the effective velocity ratio, which is defined as the ratio of the momentum flux across the jet exit to the momentum flux of the crossflow over an equal area. Since both the jet and the crossflowing air obey the same ideal gas equation of state and assuming the static pressure at the jet exit is nearly equal to the crossflow static pressure, the effective velocity ratio may be stated as $R = M_j/M_\infty$ (see Ref. 23).

Several solutions of the Reynolds averaged Navier-Stokes equations have already been computed for both single[7,24–30] and multiple jets in a crossflow.[31–33] Previous elliptic solutions of the three-dimensional Navier-Stokes equations computed

Presented as Paper 89-0448 at the AIAA 27th Aerospace Sciences Meeting, Reno, NV, Jan. 9–12, 1989; received Oct. 27, 1989; revision received Dec. 12, 1990; accepted for publication Dec. 13, 1990.

*Aerospace Engineer. Member AIAA.
†Professor, Aerospace Engineering, Mechanics and Engineering Science Department. Member AIAA.
‡Graduate Student, Aerospace Engineering, Mechanics and Engineering Science Department.

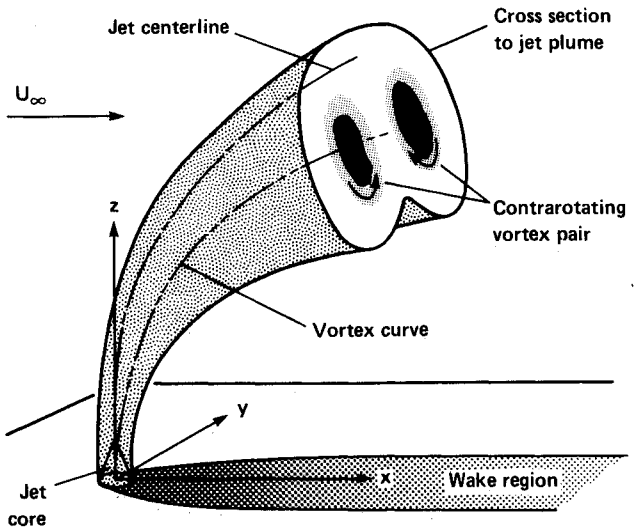

Fig. 1 Schematic of a jet in a crossflow.

on relatively coarse grids have failed to provide a detailed picture of the entire flowfield. For example, calculations of a turbulent jet by Patankar et al.[25] exhibit good agreement for the jet centerline and the rate of decay of the jet velocity, but deviate significantly from the experimental velocity profiles along the jet axis after the jet deflects and in the reversed flow region. In addition, Khan et al.[31] and Demuren[32] utilized systematic grid refinements in computing the flow induced by a row of jets and found that it was not possible to obtain grid independent results on the finest mesh tested.

Most recently, several higher-resolution computations, each employing on the order of 100,000 grid points to discretize the three-dimensional domain, have been reported. A detailed picture of the jet plume and a discussion of the vorticity dynamics for a turbulent jet with jet-to-crossflow velocity ratios between 2 and 8 is given by Sykes et al.[27] However, since their primary motivation is the behavior of jets remote from a wall, they do not attempt to resolve details of the wake region. A steady, laminar calculation for a jet and its wake at a velocity ratio of 8 by Harloff and Lytle[30] does not show satisfactory agreement with experiment for the jet centerline or the vortex trajectory.

The present research is directed toward evaluating the fluid mechanics of a jet in a crossflow on a refined computational mesh with a particular emphasis placed on characterizing the contrarotating vortex pair. In this paper, a brief description of the numerical approach, including the computer code, the computational grid, and the boundary conditions, is given and numerical results are presented. When experimental measurements are available, quantitative comparisons are made between the calculated and measured data for the jet trajectory, the plate pressure distribution, and the properties of the contrarotating vortex pair. Visualization of the computed results on a graphics workstation is used to provide insight into the physics of this three-dimensional flowfield.

Numerical Approach

Numerical Algorithm

The numerical scheme selected is contained in the general purpose simulation code designated F3D.[34] It solves the thin-layer Navier-Stokes equations cast in generalized coordinates and written in conservation law form. The numerical algorithm incorporates two implicit factors and partial flux splitting. Flux splitting[35] and upwind differencing are used for the convection terms in the freestream ξ direction, whereas central differencing is applied in the remaining spatial directions η and ζ. This implicit, two-factored scheme is shown to be unconditionally stable for a model scalar wave equation.[36] In order to control nonlinear instabilities, a combination of second- and fourth-order differences is added as smoothing in the centrally differenced directions.[34] Numerical dissipation is also added in the upwind direction, in this case through the flux splitting. The F3D code has second-order spatial accuracy.

For the steady calculations considered here, a space-varying time step is used to accelerate convergence.[37] This time step depends on the local grid spacing and renders the calculation non-time-accurate. For laminar calculations, the coefficient of viscosity μ is obtained from Sutherland's law. The code, which is fully vectorized for supercomputers, requires 10^{-4} CPU s/iteration/grid point on the CRAY-2 computer.

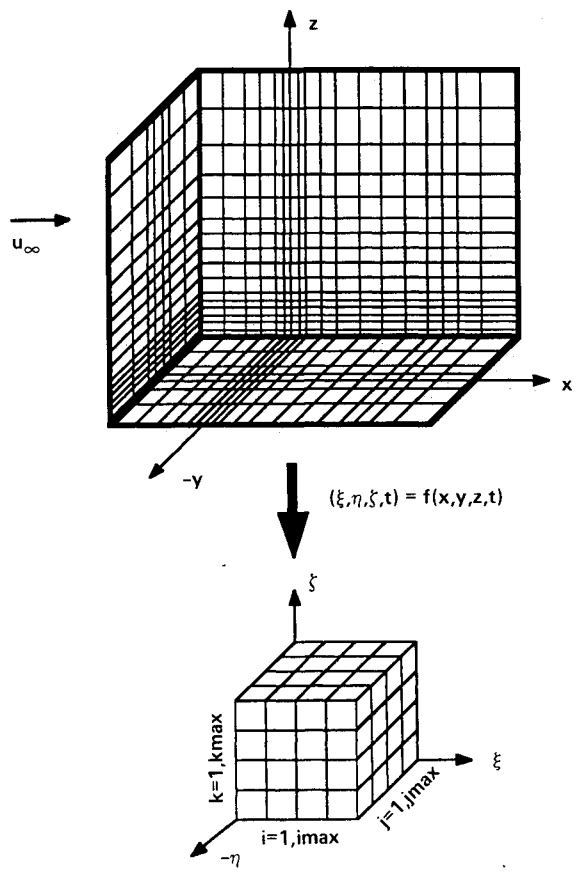

a) Physical and computational space

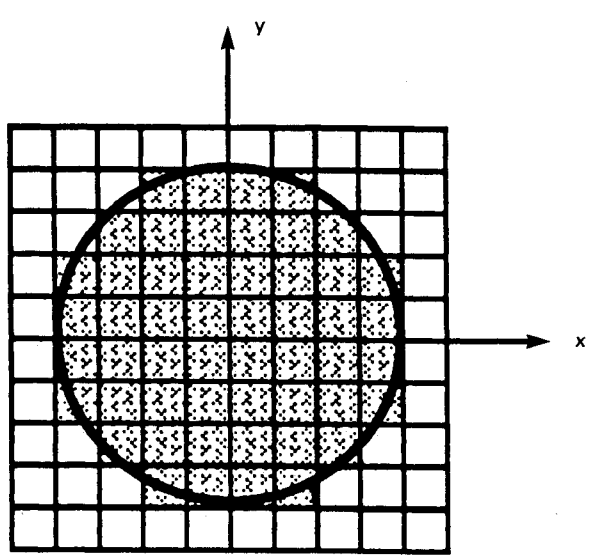

b) Jet exit grid

Fig. 2 Grid structure.

Computational Grid

A three-dimensional grid, shown in Fig. 2a, is set up for the calculations. A right-handed Cartesian coordinate system is used with x increasing in the freestream direction and z pointing away from the plate. The rectangular grid is exponentially clustered within the boundary layer of the flat plate and around the jet exit, which is centered at the origin of the Cartesian coordinate system. For calculations, the physical domain is transformed to a computational space with uniform grid spacing, as shown in Fig. 2a. The computational variables ξ, η, ζ, and τ are functions of the Cartesian coordinates x, y, z, and t. In the transformed grid system, ξ corresponds to the freestream direction such that $\xi_{\min}$ coincides with the upstream boundary where $x = x_{\min}$, η spans the domain laterally, and ζ is the direction normal to the body surface such that $\zeta_{\min}$ maps to the solid surface.

Since the experimental measurements to be used in the comparisons are for jets exhausting through a circular orifice, the jet exit is approximated by a right-angled polygon of nearly equal area in the Cartesian grid system, as shown in Fig. 2b. Although the relatively sparse experimental measurements indicate that the global features of the flow induced by a jet in a crossflow are steady and symmetric, no symmetry assumptions are made for the computational domain. Nevertheless, in accord with previous experimental studies, the $y = 0$ plane is referred to as the symmetry plane.

Initial calculations are made on a relatively coarse grid with 39 (freestream) $\times$ 35 (normal to the $y = 0$ plane) $\times$ 32 (normal to the flat plate) points. The coarse grid computations are made on a GRAY-XMP computer. In order to investigate the effects of the grid on the computation, the grid density is increased from 39 $\times$ 35 $\times$ 32 (43,680 points) to 55 $\times$ 55 $\times$ 50 (151,250 points). The minimum grid spacing in the freestream and lateral directions is 0.125 jet diameters. The finest mesh spacing normal to the plate is 0.005 jet diameters. Details of the grid structure are stated by Roth.[7] Calculations on the refined grids required approximately 12 h CPU on the CRAY-2 computer.

Boundary Conditions

The boundary conditions that are used for the jet in a crossflow problem with the previously described grid topology are the following: 1) freestream conditions on the upstream boundary $\xi_{\min}$; 2) extrapolation on the downstream boundary $\xi_{\min}$, such that

$$\boldsymbol{Q}^{t+1}_{i\max,j,k} = 2\boldsymbol{Q}^{t}_{i\max-1,j,k} - \boldsymbol{Q}^{t}_{i\max-2,j,k}$$

where $\boldsymbol{Q}$ is a vector containing the conservative variables, $i$max corresponds to the $\xi_{\min}$ plane, and t refers to the time level; 3) zero normal flow gradients on the lateral surfaces $\eta_{\min}$ and $\eta_{\max}$; 4) no-slip velocity conditions on the flat plate $\zeta_{\min}$ and $x^2 + y^2 > 0.25$; 5) jet exit profile for $x^2 + y^2 \leq 0.25$ and $\zeta_{\min}$; and 6) freestream conditions for the top surface $\zeta_{\min}$. In general, these conditions are implemented explicitly in modular form within the code.

Three-dimensional mean flow and turbulence measurements at the jet exit for flows with effective velocity ratios <3 are presented by Andreopoulos[19] and Andreopoulos and Rodi.[20] Their results indicate that, at low velocity ratios, the jet flow is affected up to 3 jet diameters upstream of the pipe exit by the crossflow, but this distortion diminishes as the velocity ratio is increased. The precise physical boundary condition at the jet exit, for the jet and freestream conditions investigated here, has not been measured. Previous authors have imposed the jet exit condition by specifying uniform vertical velocity[25,27] or uniform total pressure[31,32] or by initiating the calculation inside the jet supply pipe.[33] In this simulation, a uniform velocity profile jet is injected from the lower boundary into the flowfield. This simplifying assumption may lead to discrepancies between the computed and measured results.

Results and Discussion

The computational cases, which were chosen to correspond with the wind-tunnel tests of Fearn and Weston,[17,23,38,39] are summarized by the effective velocity ratio in Table 1. The numerical results are computed on the three-dimensional computational grid described in the previous section, which has the grid density and the domain limits given in Table 1. In order to investigate the effects of the domain size on the solutions, computations were also made for the case $R = 6$ with the domain limits extended by 20–25% in each direction; no significant variation was found for the jet deflection, the flow direction at the top and lateral boundaries, or the plate pressure distribution.

In the measured flows, both the jet and the freestream flow are turbulent; however, no turbulence modeling is used in this numerical model. In experimental studies of flows with relatively low velocity ratios, both Crabb et al.[3] and Andreopoulos[19] found regions in which the turbulence field is anisotropic, which suggests that the commonly used turbulence models, such as eddy viscosity and k-ε models, will not be able to account for all of the features of the flow. Thus, the exclusion of turbulence from the calculation permits the evaluation of the numerical model without having to estimate the errors associated with an inadequate turbulence model.

Complete quantitative agreement between the measured turbulent flow and the calculated flow cannot be anticipated since, for example, boundary-layer velocity profiles and separation point locations are dependent on the characteristics of the boundary layer. However, the effective velocity ratio is the primary variable determining the global features of the jet such as the jet centerline, the contrarotating vortex pair, and the plate pressure distribution. The computed results indicate that these features are captured reasonably well in a laminar simulation.

In the jet in a crossflow problem, the use of the thin-layer equations allows the physically correct boundary condition to be enforced on the plate, but their application must be viewed with caution. The thin-layer approximation takes advantage of the observation that, for many high Reynolds number flows, the viscous effects are confined to a relatively thin region near a solid boundary. Within the thin layer, high gradients are found in only one direction, normal to the surface. Thus, the thin-layer Navier-Stokes equations are computationally advantageous in comparison with full Navier-Stokes methods since all viscous terms containing derivatives that are parallel to the body surface are neglected and a highly clustered mesh is required to resolve diffusive terms in only one direction.[40] The jet in crossflow contains high flow gradients in all three directions. Further, the flowfield contains curvature and a three-dimensional, separated wake region. Although the high gradients perpendicular to the plate within the boundary layer may be captured, the thin-layer approximation becomes inadequate in other regions of the flow, such as the shear layer between the jet and the crossflowing fluid and the wake region. Even under such restrictions, the key features of the flow are captured.

Computed Flow in the Symmetry Plane

Selected velocity vectors in the symmetry plane for the high resolution $R = 4$ case are presented in Fig. 3a. The vector plot shows the onset flow, the deflected jet plume, a reversed flow region behind the jet, an upwash velocity component

Table 1 Summary of computational cases

R	M_∞	Re	Grid size	$x_{\min}$	$x_{\max}$	$y_{\max}$	$z_{\max}$
4	0.20	500,000	39 × 35 × 32	−5.0	15.0	9.5	18.0
4	0.19	500,000	55 × 55 × 50	−6.0	15.0	9.5	18.0
6	0.13	350,000	39 × 35 × 32	−5.0	15.0	9.5	18.0
6	0.13	350,000	55 × 55 × 50	−6.0	15.0	9.5	18.0
8	0.12	350,000	39 × 35 × 32	−5.0	15.0	10.0	20.0

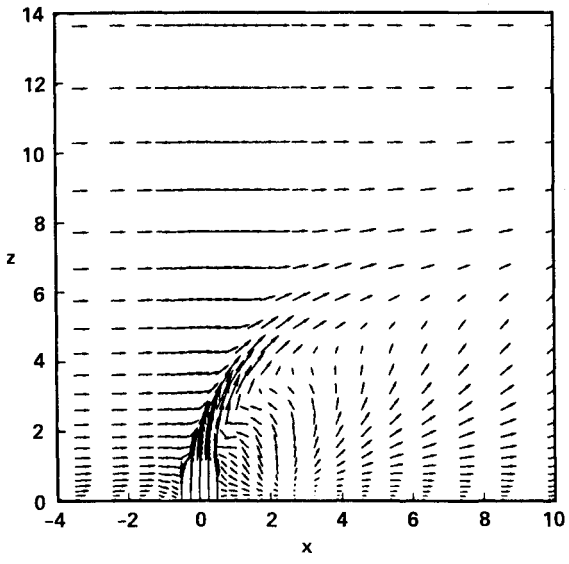

a) Velocity vectors

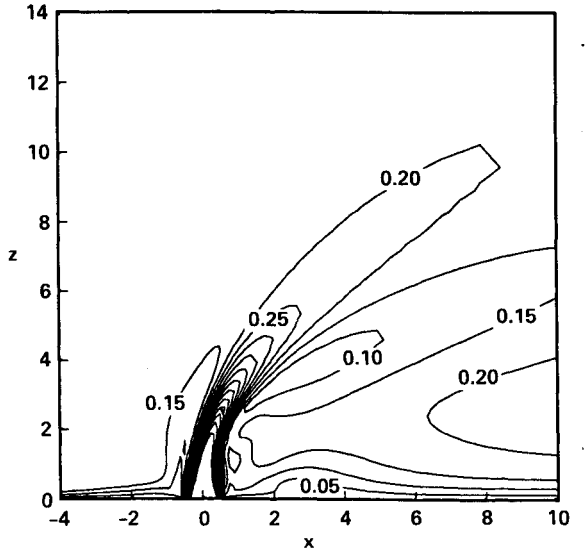

b) Mach contours: minimum 0.05; maximum 0.75; and increment 0.05

Fig. 3 Symmetry plane flow for $R = 4$.

that lies in the symmetry plane between the contrarotating vortices sketched in Fig. 1, and, finally, the predominantly stream-wise flow. The computed velocity field correlates reasonably well with the symmetry plane velocity measurements presented by Fearn and Weston[17,38,39] and by Fearn and Benson[41] with the exception of the region located behind the jet plume at approximately $x = 1.5$. In this region, computed velocity vectors are rotated counterclockwise by angles up to 90 deg. This behavior is observed for all effective velocity ratios computed but tends to be less apparent in the coarse grid solutions in which numerical diffusion is increased. It is concluded that the computed flow behavior is related to the jet entrainment rate.

In the region close to the flat plate and immediately preceding the jet orifice, the velocity vectors have a downward component, which suggests the presence of a weak flow separation. Flow measurements and visualization have shown that a separated flow region dominated by a horseshoe vortex system is buried within the boundary layer upstream of the jet exit.[19-21,42] The flow separation and formation of the horseshoe vortex system are primarily due to the adverse pressure gradients and the deflection of streamlines caused by the blockage effects of the jet. The detailed structure of the horseshoe vortex system depends on the plate boundary-layer profile and unsteadiness as well as the effective velocity ratio.[21] Thus, with the numerical model constraints, these fine-scale flow features cannot be fully resolved.

The deflection and penetration of the jet plume are illustrated clearly in the plot of Mach number contours shown in Fig. 3b for the $R = 4$ jet. The small, nearly triangular contours located just above the jet exit denote a region of high velocity. This region, which reaches approximately 2 jet diameters into the flow, is part of the jet core that is identified in Fig. 1. The velocity field exhibits relatively slow changes within the jet core in comparison with the high velocity gradients found in the shear layer that exist at the interface between the jet and the crossflowing fluid. Distortion, caused by the crossflow, and rapid diffusion by the shear layer eventually erode the jet core.

Vertical profiles of the freestream velocity component in the symmetry plane at downstream locations of $x = 2.0$, 4.0, and 8.0 are shown in Fig. 4 for the $R = 4$ cases. The location of the jet centerline is closely approximated by the point of maximum freestream velocity component. In Fig. 4, the maximum velocity peaks are more pronounced or tend to be greater in magnitude on the fine grid than on the coarse grid. Although these peaks do not reflect the same magnitude, in

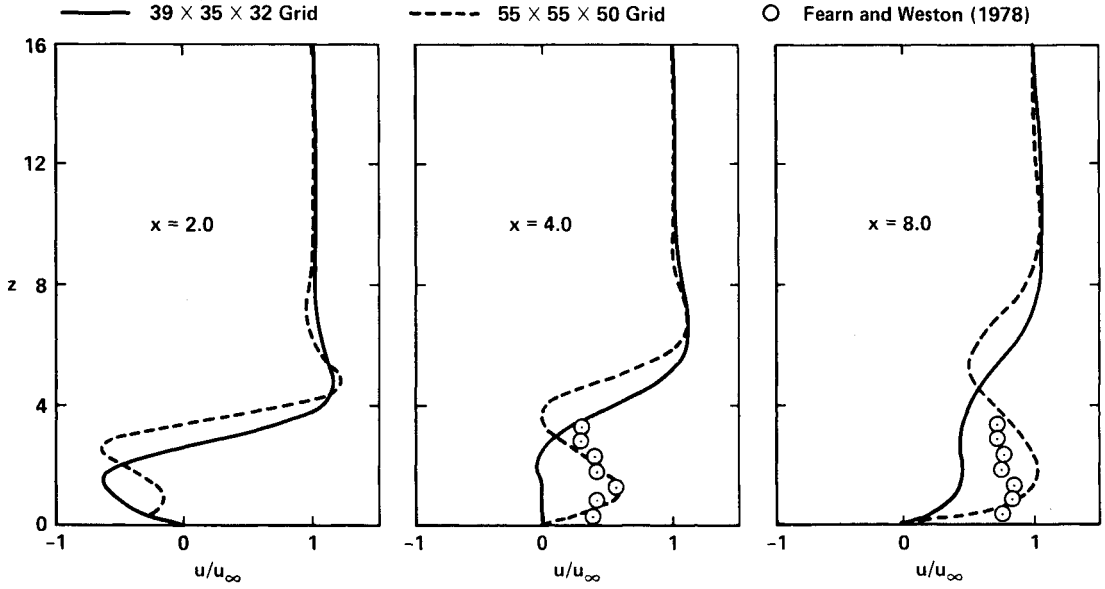

Fig. 4 Comparison of streamwise velocity profiles in the symmetry plane for $R = 4$.

general, their vertical locations agree well. At the most downstream location, this difference is minimized due to the increased similarity between the two clustered grids far downstream. A similar grid dependence was found by Khan et al.[31] and Demuren.[32]

As indicated in Fig. 4, the coarse and fine grid results vary as much as 50% in the wake region, within 3 jet diameters of the flat plate. Both solutions show a region of reversed flow, but the numerical dissipation is increased and the boundary layer is not resolved on the coarse grid. The experimental measurements[38] that are plotted for the planes $x = 4.0$ and 8.0 in Fig. 4 show that the fine grid solution more accurately characterizes the flow in the wake region. Although this discussion pertained to $R = 4$, similar conclusions are valid for $R = 6$ (see Ref. 7).

Jet Centerline

The jet centerline is defined to be the locus of points of maximum velocity in the direction of the jet in the plane of symmetry. In all of the cases examined, the computed centerline compares favorably with Fearn and Weston's experimental data and with the empirically predicted jet centerline.[17] This agreement is demonstrated in Fig. 5 using the data for the most refined grids. Only small deviations occur between the jet paths computed on the coarse grid and the paths calculated on the fine grid, which indicates that the jet centerline may be captured with a relatively small number of grid points. Furthermore, for the $R = 4$ cases, inviscid computations were also made. The computed jet trajectories are nearly indistinguishable for the viscous and inviscid predictions. This agreement shows that pressure, rather than viscosity, is the primary mechanism governing the initial deflection of the jet.

The decay of the jet centerline speed for $R = 4$ is shown in Fig. 6. For this velocity ratio, the computational results show greater jet penetration and a more rapid velocity decay than the experimental results.

Plate Pressure Distribution

A comparison of the calculated and experimental pressure coefficients C_p on the flat plate for the jet $R = 4$ is made in the contour plot shown in Fig. 7. Contours of constant pressure coefficient for the high resolution $R = 4$ computation are plotted in the lower half plane in Fig. 7. The upper half plane shows the corresponding contours from the experimental data.[23] It is noted that, in regions of low pressure gradients,

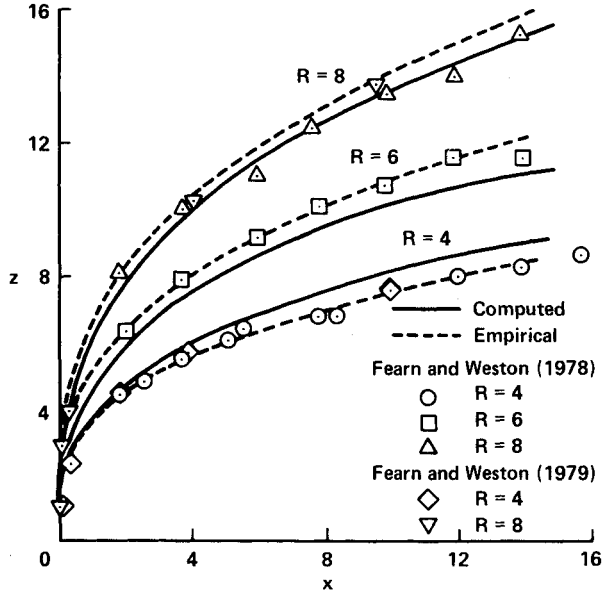

Fig. 5 Computed, experimental, and empirical jet centerline for $R = 4$, 6, and 8.

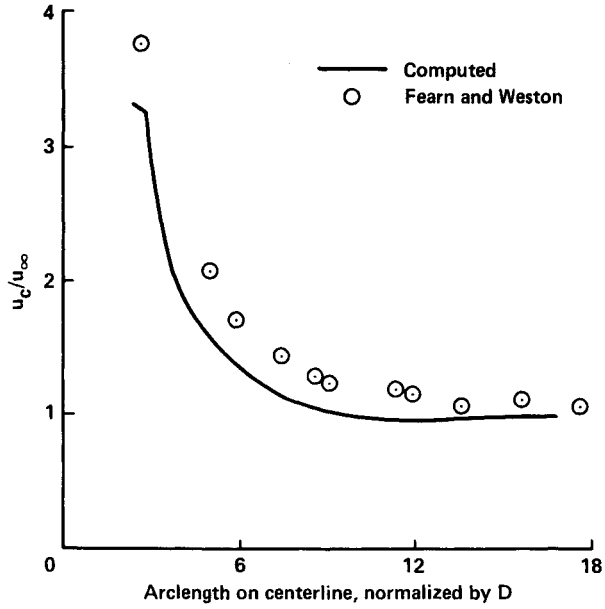

Fig. 6 Velocity decay along the jet centerline for $R = 4$.

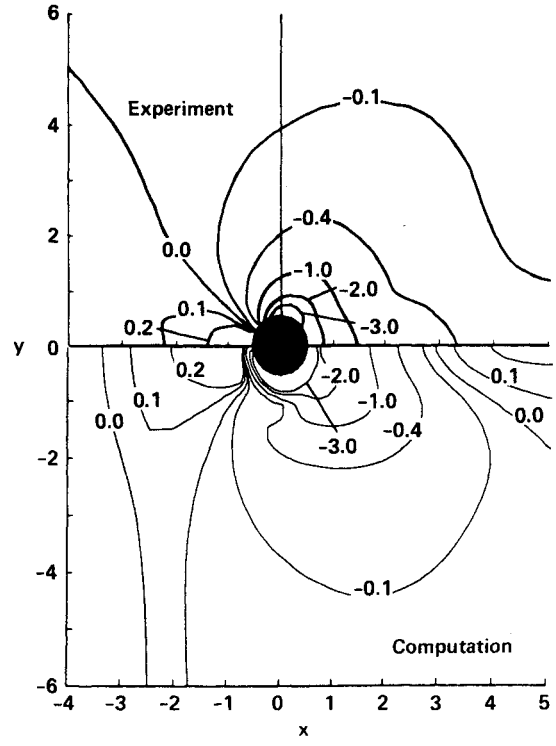

Fig. 7 Constant pressure contours on the plate for $R = 4$.

the experimental contours have an error band of up to 1 jet diameter.[23] The largest discrepancy between the calculated and measured pressures occurs near the interface between the jet and the crossflowing fluid. The numerical inaccuracy may be induced by the constant velocity jet exit boundary condition imposed in this simulation.

The following flow characteristics are evident from the pressure distribution. First, upstream of the jet exit, there is a positive pressure gradient. This high pressure region is similar in area to the positive pressure region upstream of a solid blockage of the same diameter.[13] Next, the largest pressure gradient occurs close to the side of the jet with the region of minimum pressure centered approximately 135 deg from the negative x axis. Although there are also low pressures at the side of a solid blockage,[13] the minimum pressure coefficient for potential flow around a solid cylinder is only -3 and occurs along $x = 0$. Thus, the low pressures near the side of

the jet are probably due to entrainment and the presence of the contraordinating vortices near the base of the jet. Finally, the calculated pressures in the wake are, in general, higher than the measured pressures.

Examination of the plate pressure distribution for a jet in a crossflow shows a positive pressure region upstream and a larger region of negative pressures to the side and downstream of the jet. If a similar pressure distribution is induced on the surface of a STOVL aircraft by the lift jets, it is evident from the contours that the lift would be negative. Further, the positive upstream pressures and the negative downstream pressures will create a nose-up pitching moment on the aerodynamic surface. Both of these trends are also noted for STOVL aircraft.[1]

Flow in Cross Sections

The most natural way to examine the contrarotating vortex pair is in a cross section that is oriented perpendicular to the jet plume. A cross section is described by specifying its inclination angle φ, measured in degrees from the negative z axis, and the (x,z) location of the origin of the cross-section coordinate system in the $y = 0$ plane. For examination, the computed flow variables are interpolated onto a uniform mesh in the cross-section plane and resolved into the local coordinate system.

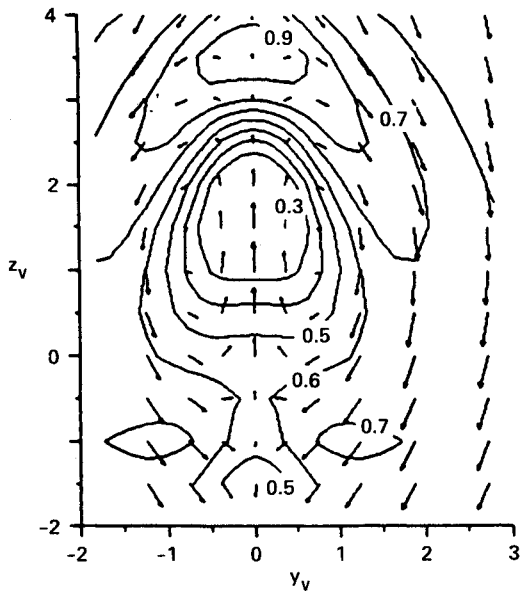

a) Computation, $u_c/u_\infty = 1.47$

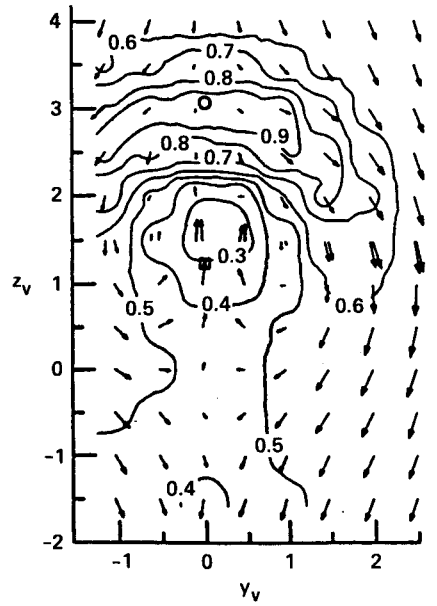

b) Fearn and Weston[38] $u_c/u_\infty = 1.62$

Fig. 8 Flow in a cross section perpendicular to the jet plume: contours of constant u_v/u_c are superimposed on the vectors $(v_v + w_v)/u_c$ for $R = 4$; $(x,z) = (4.16, 2.03)$; $\varphi = 32$ deg.

The computed velocity field for one cross section for $R = 4$ is shown in Fig. 8a and the experimental results of Fearn and Weston[38] are shown in Fig. 8b. The inclination angle is $\varphi = 32$ deg and the origin of the cross-section coordinate system is located at $(x,z) = (4.16, 2.03)$. The velocity component perpendicular to the cross section is presented as contours of constant u_v/u_c where u_c is the jet centerline speed given for the cross section. At selected points within the cross section, the projection of the velocity vector onto the cross section, $(v_v + w_v)/u_c$, is presented.

The cross-section velocity plots show the flow structure in the jet plume, and although there are differences in detail, it is evident that the computation is describing the major features of this flow structure. The contours show some of the extent of the jet plume and exhibit the characteristic kidney shape attributed to a jet in a crossflow. In addition, these contours can be used to locate the jet centerline. The velocity vector projections indicate that a pair of contrarotating vortices is a significant feature of the flow.

Diffuse Vortex Method

The computed velocity field is analyzed using the diffuse vortex method described by Fearn and Weston[17] so that a comparison of the global vortex properties can be made between the computation and the experiment. In the diffuse vortex method, it is assumed that each vortex is composed of a Gaussian distribution of vorticity. Then, the location, strength and diffuseness of the vortex pair are determined from all of the input upwash velocities within a vortex cross section. The diffuse vortex method is a two-dimensional model and only describes the vorticity component that is perpendicular to the cross section. Thus, the numerical values that are inferred for the vortex parameters should be considered as a rough description of the streamwise vorticity. In the region of the jet plume far from the jet exit, the results of the diffuse vortex method are not sensitive to relatively small changes in the cross-section angle.

The results of the diffuse vortex method analysis for several vortex cross sections are displayed graphically in Figs. 9 together with the results of Refs. 17 and 41. The vortex penetration for $R = 4$ and 6 is shown in Fig. 9a. Figure 9b presents the vortex half-spacing, and Fig. 9c presents the vortex strength. The vortex strength is nondimensionalized by the value obtained for a roll-up of the vorticity associated with two-dimensional potential flow around a circular cylinder, into a contrarotating vortex pair as described by Chang.[43]

The vortex penetration curves for both the $R = 4$ and 6 jets computed on the fine grid are within 30% of a jet diameter of the experimental curve. In each case, the curve for the computed data is closer to the plate than the experimental curve and shows less curvature. Further, the computed data predicts that the vortices have less separation than in the experiment, as indicated by the lower, flatter curves in Fig. 9b. Although the vortex penetration is highly dependent on the effective velocity ratio, the vortex separation is only weakly related to it. In addition to being closer together and closer to the plate, the vortex strength plotted in Fig. 9c for the computed flows is approximately 10% below the vortex strength that was inferred for the experiment at $x = 3.0$ and is nearly 40% greater than the experiment at $x = 10.0$.

Examination of Fig. 9a–c shows that grid resolution affects the properties of the contrarotating vortex pair. In short, the $R = 4$ coarse grid solution is more diffuse than both the experimental flow and the fine grid computation. Although the numerical diffusion is reduced as the mesh is refined, either turbulence modeling is needed to adjust the diffusion

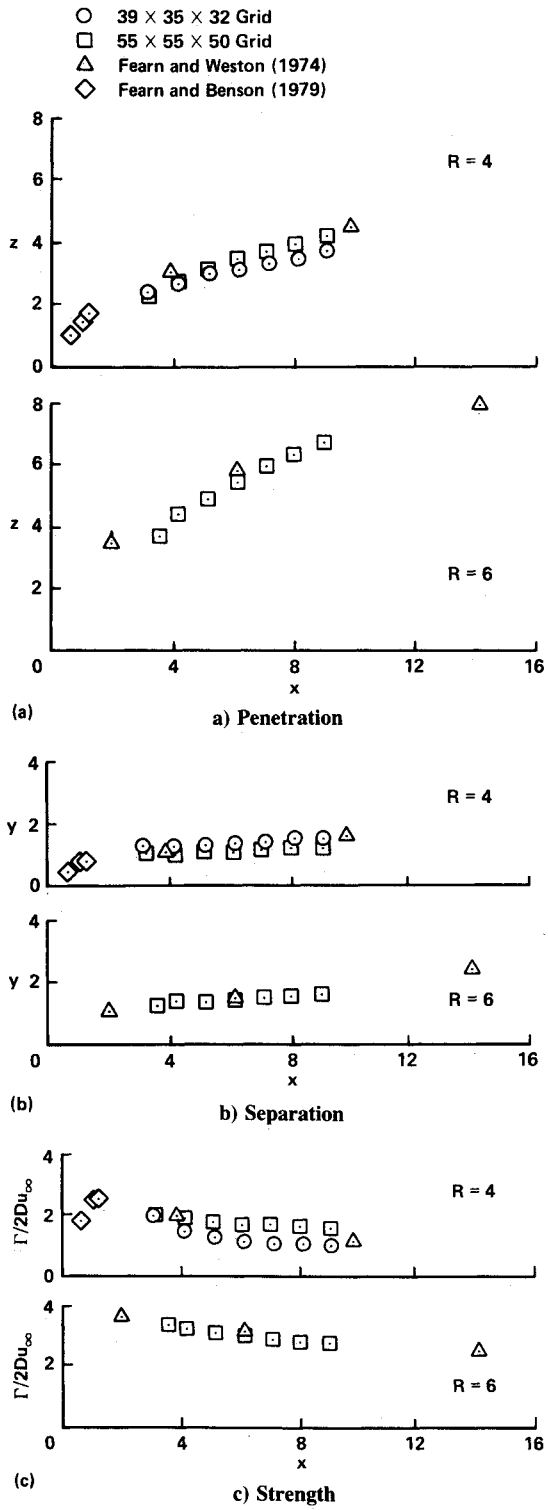

Fig. 9 Properties of the contrarotating vortex pair.

rate or some of the viscous terms that are neglected in the thin-layer assumption must be included in the calculation to provide better agreement with the physical flow.

Flow Visualization

Streamlines

Flow visualization of the computed results is accomplished by constructing particle traces on a graphics workstation. For steady flows, particle traces or equivalently, three-dimensional streamlines, are computed by releasing a particle that moves with the local fluid velocity originating from selected spatial locations. The computed streamlines for the case R = 6 are shown in Fig. 10a. Particles are released both upstream of the jet within the boundary layer at a height of 0.005 D and from within the jet exit itself.

Fluid from the jet exit, which will be referred to as jet fluid, exhausts into the flowfield and is deflected by the freestream. The fluid on the upstream part of the jet undergoes rapid, viscous interaction with the freestream. In contrast, the fluid on the aft part follows a more vertical trajectory before being deflected. The pressure imbalance resulting from the relatively high pressure upstream of the jet and the low pressure wake region behind the jet contributes to the curvature of the streamlines. It is interesting to note that the streamline emanating from the center of the jet orifice coincides with the jet centerline computed using the definition stated earlier in this paper. This confirms that the jet trajectory determined through flow visualization techniques, such as the water injection method used by Margason,[10] corresponds closely to the jet centerline.

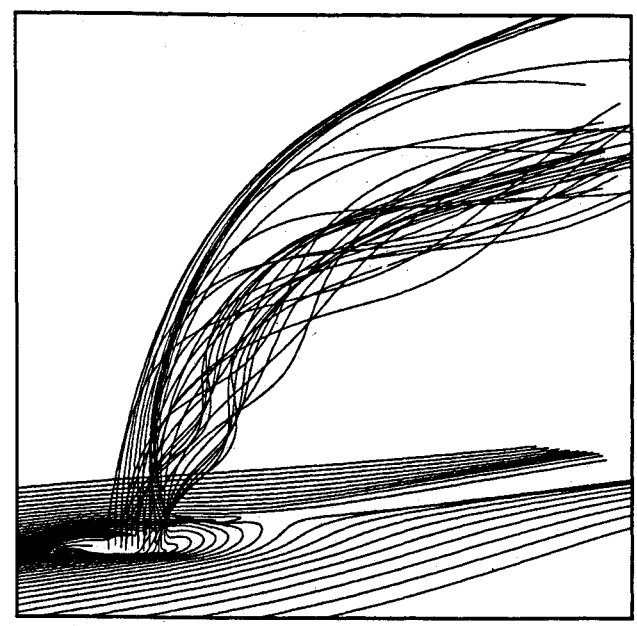

a) Particles are released within the boundary layer upstream of the jet and within the jet exit

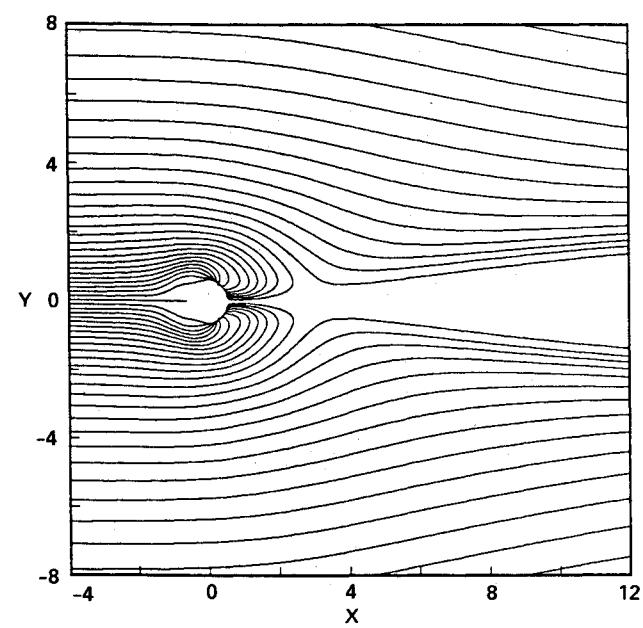

b) Surface streamlines at height 0.005 D

Fig. 10 Particle traces for R = 6.

The boundary-layer fluid approaches the jet, moves around it staying relatively close to the plate, and some of the fluid is swept up into the aft side of the jet plume, which consists of the original jet fluid together with entrained boundary-layer and freestream fluid. The boundary-layer fluid that reverses and moves between the two vortex cores is drawn into the low pressure region in the jet plume close to the aft side of the jet. Finally, some of the deflected boundary-layer fluid continues moving downstream before being caught up in the jet plume. This feature is emphasized in flow visualization studies by ONERA.[16]

Surface Streamlines

Surface streamlines are constructed by restricting particles to the plane just above the flat plate; that is, the normal velocity component is set to zero during the time integration. These surface streamlines, which are analogous to the surface shear stress lines that are seen in surface oil flow visualization experiments, describe the steady flow characteristics within the boundary layer of the plate. In Fig. 10b, the surface streamlines taken at a height 0.005 D above the plate for $R = 6$ are shown. The freestream flow decelerates upstream of the jet exit due to the presence of the jet and then accelerates around the jet. Some of the surface streamlines bend in toward the jet and seem to terminate at the edge of the orifice. Other streamlines are deflected around the jet periphery and into the boundary of the wake region downstream of the jet exit. Within the wake region, some fluid moves upstream, toward the jet exit. Directly behind the reverse flow region, wake flow moves away from the jet and into the wake boundary, which may consist of a horseshoe vortex formed around the jet core. Further details of the surface flow topology are examined in Ref. 7.

Conclusions

The accuracy of a three-dimensional, thin-layer Navier-Stokes code applied to a jet in a crossflow was evaluated through comparisons with experimental measurements. It was found that the jet centerline can be predicted accurately with a small number of grid points and is relatively insensitive to viscous effects. With the exception of rapid pressure recovery in the wake, the general trends of the plate pressure distribution matched the experiment. Overall, reasonable agreement was demonstrated between the computation and the experiment for the vortex strength, location, and diffusivity calculated using the diffuse vortex method. The flow visualization showed that the jet centerline is comprised primarily of original jet fluid, whereas the cores of the contrarotating vortices contain fluid that originated within the flat plate boundary layer as well as jet and freestream fluid. This method provides an adequate model for the global characteristics of the flowfield but is not capable of describing finer scale flow features such as the upstream separation vortex or the detailed wake structure, which would require grid refinements, full Navier-Stokes equations, and turbulence modeling.

References

[1]Margason, R. J., and Fearn, R. L., "Jet-Wake Characteristics and Their Induced Aerodynamic Effects on V/STOL Aircraft," NASA SP-218, Sept. 1969.

[2]"Analysis of a Jet in a Subsonic Crosswind," NASA SP-218, Sept. 1969.

[3]Crabb, D., Durao, D. F. G., and Whitelaw, J. H., "A Jet Normal to a Crossflow," Imperial College, London, England, UK, Rept. FS/78/35, March 1979.

[4]Spee, B. M., "Technical Evaluation Report on the AGARD Fluid Dynamics Panel Symposium on Fluid Dynamics of Jets with Applications to V/STOL," AGARD Advisory Rept. No. 187, July 1982.

[5]Hancock, G. J., "A Review of the Aerodynamics of a Jet in a Cross Flow," *Aeronautical Journal*, Vol. 91, No. 905, 1987, pp. 201–213.

[6]Margason, R., and Kuhn, R., "Application of Empirical and Linear Methods to VSTOL Powered-Lift Aerodynamics," Society of Automotive Engineers, Paper 872341, Dec. 1987.

[7]Roth, K. R., "Application of a Three-Dimensional Navier-Stokes Method for a Subsonic Jet in a Crossflow," Ph.D. Dissertation, University of Florida, Gainesville, FL, Dec. 1988.

[8]Callaghan, E. E., and Ruggeri, R. S., "Investigation of the Penetration of an Air Jet Directed Perpendicularly to an Air Stream," NACA TN 1615, June 1948.

[9]Jordinson, R., "Flow in a Jet Directed Normal to the Wind," British Aeronautical Research Council, Technical Rept., Reports and Memoranda 3074, Aug. 1964.

[10]Margason, R. J., "The Path of a Jet Directed at Large Angles to a Subsonic Free Stream," NASA TN D-4919, Nov. 1968.

[11]Thompson, A. M., "The Flow Induced by Jets Exhausting Normally from a Plane Wall into an Airstream," Ph.D. Dissertation, University of London, London, England, UK, 1971.

[12]Kamotani, Y., and Greber, I., "Experiments on a Turbulent Jet in a Cross-Flow," *AIAA Journal*, Vol. 10, No. 11, 1972, pp. 1425–1429.

[13]Vogler, R. D., "Surface Pressure Distributions Induced on a Flat Plate by a Cold Air Jet Issuing Perpendicularly From the Plate and Normal to a Low-Speed Free-Stream Flow," NASA TN-1629, March 1963.

[14]Bradbury, L. J. S., and Wood, M. N., "The Static Pressure Distribution Around a Circular Jet Exhausting Normally from a Plane Wall into an Airstream," British Aeronautical Research Council, CP 822, Aug. 1964.

[15]Wu, J. C., Mosher, D. K., and Wright, M. A., "Experimental and Analytical Investigations of Jets Exhausting into a Deflecting Stream," AIAA Paper 69-223, Feb. 1969.

[16]"O.N.E.R.A. Motion-Picture Film No. 575: Flows with Large Velocity Fluctuations," 35mm film published by Office National D'Études et de Recherches Aerospatiale (ONERA), Chatillon, France, 1968.

[17]Fearn, R. L., and Weston, R. P., "Vorticity Associated with a Jet in a Crossflow," *AIAA Journal*, Vol. 12, No. 12, 1974, pp. 1666–1671.

[18]Moussa, Z. M., Trischka, J. W., and Eskinazi, S., "The Near Field in the Mixing of a Round Jet with a Cross-stream," *Journal of Fluid Mechanics*, Vol. 80, Pt. 1, 1977, pp. 49–80.

[19]Andreopoulos, J., "Measurements in a Jet-Pipe Flow Issuing Perpendicularly into a Cross Stream," *Journal of Fluids Engineering*, Vol. 104, Dec. 1982, pp. 493–499.

[20]Andreopoulos, J., and Rodi, W., "Experimental Investigation of Jets in a Crossflow," *Journal of Fluid Mechanics*, Vol. 138, 1984, pp. 93–127.

[21]Krothapalli, A., Lourenco, L., and Buchlin, J. M., "The Structure of the Separated Flow Region Upstream of a Jet in a Cross Flow," AIAA Paper 89-0571, Jan. 1989.

[22]Fearn, R. L., "Progress Towards a Model to Describe Jet/Aerodynamic-Surface Interference Effects," *AIAA Journal*, Vol. 22, No. 6, 1984, pp. 752–753.

[23]Fearn, R. L., and Weston, R. P., "Induced Pressure Distribution of a Jet in a Crossflow," NASA TN D-7616, July 1975.

[24]Chien, C. J., and Schetz, J. A., "Numerical Solution of the Three-Dimensional Navier-Stokes Equations with Application to Channel Flows and a Bouyant Jet in a Cross-Flow," *Journal of Applied Mechanics*, Vol. 42, Sept. 1975, pp. 575–579.

[25]Patankar, S. V., Basu, D. K., and Alpay, S. A., "Prediction of the Three-Dimensional Velocity Field of a Deflected Turbulent Jet," *Journal of Fluids Engineering*, Vol. 99, No. 4, 1977, pp. 758–762.

[26]Baker, A. J., Orzechowski, J. A., Manhardt, P. D., and Yen, K. T., "A Three-Dimensional Finite Element Algorithm for Prediction of V/STOL Jet-Induced Flowfields," AGARD-CP-308, Oct. 1981.

[27]Sykes, R. I., Lewellen, W. S., and Parker, S. F., "On the Vorticity Dynamics of a Turbulent Jet in a Crossflow," *Journal of Fluid Mechanics*, Vol. 168, July 1986, pp. 393–413.

[28]Baker, A. J., Snyder, P. K., and Orzechowski, J. A., "Three Dimensional Nearfield Characterization of a VSTOL Jet in Turbulent Crossflow," AIAA Paper 87-0051, Jan. 1987.

[29]Roth, K. R., "Numerical Simulation of a Subsonic Jet in a Crossflow," Society of Automotive Engineers, Paper 872343, Dec. 1987.

[30]Harloff, G. J., and Lytle, J. K., "Three-Dimensional Viscous Flow Computations of a Circular Jet in a Subsonic and Supersonic Cross Flow," AIAA Paper 88-3703, June 1988.

[31]Khan, Z. A., McGuirk, J. J., and Whitelaw, J. H., "A Row of Jets in a Crossflow," AGARD-CP-308, Oct. 1981.

[32]Demuren, A. O., "Numerical Calculations of Steady Three-Dimensional Turbulent Jets in Cross Flow," *Computor Methods in Applied Mechanics and Engineering*, Vol. 37, May 1983, pp. 309–328.

[33]Claus, R. W., "Numerical Calculation of Subsonic Jets in Crossflow with Reduced Numerical Diffusion," AIAA Paper 85-1441, July 1985.

[34]Steger, J. L., Ying, S. X., and Schiff, L. B., "A Partially Flux-Split Algorithm for Numerical Simulation of Compressible Inviscid and Viscous Flow," *Proceedings of the Workshop on Computational Fluid Dynamics*, Workshop proceedings distributed by Institute of Nonlinear Sciences, UC Davis, Davis, CA, May 1986.

[35]Steger, J. L., and Warming, R. F., "Flux-Vector Splitting of the Inviscid Gasdynamic Equations with Application to Finite Difference Methods," *Journal of Computational Physics*, Vol. 40, No. 2, 1981, pp. 263–293.

[36]Ying, S. X., "Three-Dimensional Implicit Approximately Factored Schemes for the Equations of Gasdynamics," Ph.D. Dissertation, Stanford University, Stanford, CA, June 1986.

[37]Srinivason, G. R., Chyu, W. J., and Steger, J. L., "Computation of Simple Three-Dimensional Wing-Vortex Interaction in Transonic Flow," AIAA Paper 81-1206, June 1981.

[38]Fearn, R. L., and Weston, R. P., "Induced Velocity Field of a Jet in a Crossflow," NASA TP-1087, May 1978.

[39]Fearn, R. L., and Weston, R. P., "Velocity Field of a Round Jet in a Crossflow for Various Jet Injection Angles and Velocity Ratios," NASA TP-1506, Oct. 1979.

[40]Baldwin, B. S., and Lomax, H., "Thin Layer Approximation and Algebraic Model for Separated Turbulent Flows," AIAA Paper 78-257, Jan. 1978.

[41]Fearn, R. L., and Benson, J. P., "Velocity Field Near the Jet Orifice of a Round Jet in a Crossflow," NASA CR 152293, Dec. 1979.

[42]Foss, J. F., "Interaction Region Phenomena for the Jet in a Cross-Flow Problem," Universität Karlsruhe, Karlsruhe, West Germany, Sonderforschungsbereich (SFB) Rept. 80/E/161, Feb. 1980.

[43]Chang, H., "Aufrollung lines zylindrischen Strables durch Querwind," Ph.D. Dissertation, Göttingen, Germany, 1942.